Hindawi
Geofluids
Volume 2024, Article ID 4186113, 19 pages
https://doi.org/10.1155/2024/4186113

Research Article

Anisotropy and Energy Evolution Characteristics of Shales: A Case Study of the Longmaxi Formation in Southern Sichuan Basin, China

Liu Xiangjun, Zhuang Dalin, Xiong Jian, Zhou Yishan, Liu Junjie, Deng Chong, Liang Lixi, Ding Yi, and Jian Xuemei

State Key Lab of Oil & Gas Reservoir Geology and Exploitation, Southwest Petroleum University, Chengdu 610500, China

Correspondence should be addressed to Liu Xiangjun; 13880093092@163.com and Xiong Jian; 361184163@qq.com

Received 9 June 2023; Revised 22 September 2023; Accepted 20 December 2023; Published 12 January 2024

Academic Editor: Jinze Xu

To obtain the influence of anisotropy and energy evolution characteristics on wellbore stability, the acoustic and mechanical anisotropy characteristics of shales are studied through various experiments, including scanning electron microscopy, ultrasonic pulse transmission, and uniaxial compression experiments, with the Longmaxi Formation shale in the southern area of the Sichuan Basin as the research object. The energy evolution characteristics of the Longmaxi Formation shale under different bedding angles are analyzed. The influence of anisotropy on the wellbore stability of shale formation is discussed on this basis. The results show that the acoustic and mechanical parameters, failure mode, and energy evolution characteristics of shale have significant anisotropy. Furthermore, the P-wave and S-wave time differences decrease with an increase in bedding angle. The compressive strength and Poisson's ratio decrease first and then increase with an increase in bedding angle. Meanwhile, the elastic modulus gradually increases with an increase in bedding angle. Rock samples with different bedding angles show diverse failure modes in mechanical tests, including splitting, shear, and shear-splitting failure. The total energy and elastic energy decrease first and then increase with an increase in bedding angle. Finally, the formation anisotropy affects the wellbore stability: the higher the formation anisotropy, the more vulnerable is the wellbore to instability.

1. Introduction

With the continuous increase in energy demand and the emphasis on environmental protection, the demands on energy development are increasing, and unconventional energy sources such as shale gas are gradually being valued and developed [1]. The amount of technically recoverable shale gas resources in China's favorable shale gas areas is 21.8×10^{12} m^3. This indicates that China's shale gas exploration and development potential is large and that it can play an important role in environmental protection and China's energy security [2].

The Longmaxi Formation in the Sichuan Basin is a favorable area for the exploration and development of marine shale gas in China. Commercial extraction has been achieved in this region [3, 4]. However, wellbore instability, such as sticking and collapse, generally occurs during drilling. Importantly, this affects construction progress and increases drilling costs. Acoustic parameters are the basis for well-logging analysis, calculation of mechanical parameters, and conversion of dynamic and static parameters. Strength is an essential mechanical parameter for analyzing wellbore stability and hydraulic fracturing. In the process of shale deposition and diagenesis, the mineral type and content, sedimentary environment, and sedimentary tectonic history of rocks [5] cause large differences in the acoustic and mechanical parameters of shale across regions. In addition, within the same region, the characteristics and occurrence of shale may differ substantially [6–8]. Currently, research on the anisotropy of the Longmaxi Formation shale mainly entails stress-strain curves, fracture type evaluation, and acoustic velocity determination. Chen et al. [6] studied the mechanical characteristics and anisotropy of the black shale of the Lower Cambrian Niutitang Formation. Hou

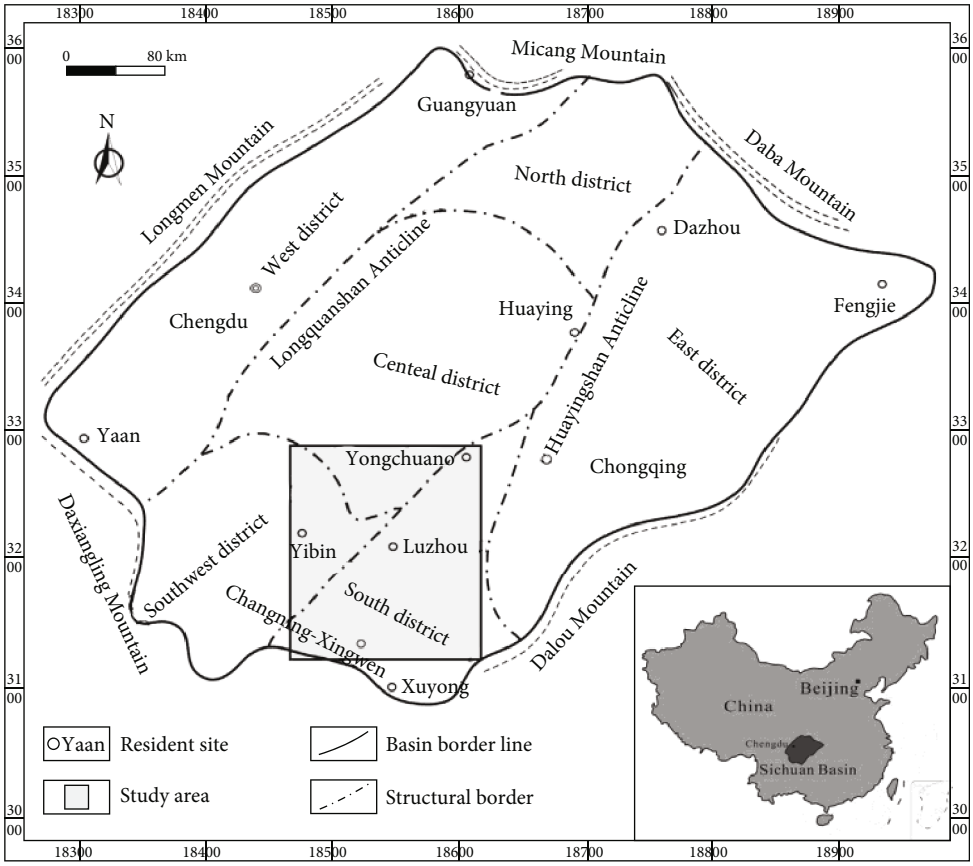

Figure 1: Geographic location and study area of Sichuan Basin [17].

et al. [8] studied the stress-strain curve and rock fracture type of the Longmaxi Formation shale in Pengshui, Chongqing, through a uniaxial compression test. Gao et al. [7] considered the Longmaxi Formation shale to analyze the variation rule of its compressive strength under the influence of different confining pressures and bedding angles. Lei et al. [9] studied the influence of bedding characteristics on shale strength parameters, elastic parameters, and fracture mode by combining physical and numerical experiments. Cui et al. [10] studied the influence of different coring angles on brittle anisotropy based on uniaxial/triaxial compression experiments with Longmaxi Formation shale as the research object. Wang et al. [11] performed mechanical experiments on Longmaxi Formation shale in the Changning area, Sichuan Basin, and studied its anisotropy through longitudinal and transverse wave tests. Chen et al. [12] studied the relationship between shale acoustic velocity, acoustic attenuation coefficient, and bedding angle using a numerical simulation method. Xu et al. [13] systematically studied the influence of the shale bedding structure on ultrasonic characteristics by using the second-order time and fourth-order space staggered-grid finite difference method. The aforementioned research results provide an important reference for understanding the variation laws of the acoustic and mechanical properties of Longmaxi Formation shale under the influence of anisotropy. Furthermore, anisotropy would also have a significant impact on the characteristics of rock energy evolution. Many studies have been conducted on the energy evolution characteristics of sandstone, coal, granite, and other types of rocks [14–16]. However, there is a deficiency of research on the influence of anisotropy on the rock energy evolution characteristics.

In this study, the Longmaxi Formation shale in the southern area of the Sichuan Basin in China is considered as the research object; the acoustic and mechanical anisotropy characteristics of shales are studied using various methods, including scanning electron microscopy (SEM), ultrasonic pulse transmission, and uniaxial compression experiments. The energy evolution characteristics of Longmaxi Formation shale with different bedding angles are analyzed. In addition, the influence of shale anisotropy on wellbore stability is discussed on this basis. This study is of guiding significance for optimizing drilling design, reducing wellbore instability, and improving production in the subsequent period.

2. Geological Settings and Samples

The Sichuan Basin is one of the most important oil- and gas-bearing basins in China. It is located in the southwest of China to the west of the Yangtze River basin and covers an area of over 1.81×10^4 km^2 (Figure 1) [17]. The substantiated natural gas reserves in Sichuan Basin total 8.40×10^{12} m^3. The annual outputs of natural gas and crude oil are

1.20×10^{11} m^3 and 1.45×10^5 t, respectively [18]. Fuling, Weirong, Weiyuan, Changning, Zhaotong, and other national shale gas demonstration zones have been identified and established in the Basin and surrounding areas [19]. The Sichuan Basin is a complex superimposed basin located in the northwest edge of the Yangtze paraplatform. It extends to the Chuanxiang fault fold belt in the east, Longmen Mountain fault fold belt in the west, Micang Mountain–Daba Mountain fault fold belt in the north, and Emei Washan fault block belt and Loushan fold belt in the south. It can be divided into six secondary structural belts: the North Sichuan low and gentle structural belt, East Sichuan high and steep structural belt, Central Sichuan flat and gentle structural belt, West Sichuan low and steep structural belt, Southwest Sichuan low and steep structural belt, and South Sichuan low and steep structural belt [20]. The Longmaxi Formation shale is widely distributed in most areas of the Sichuan Basin, with a large shale deposition thickness and stable distribution. The Longmaxi Formation shale in the southern area of the basin has a thickness range of 229.2–672.5 m. The cumulative deposition thickness of the high-quality shale section at the bottom is 50–85 m [18].

The experimental rock samples in this article were taken from the shale of the Longmaxi Formation in the southeastern Sichuan Basin. According to the *GB/T 50266—2013 Test Method Standard for Engineering Rock Mass* [21], rock samples with different bedding angles were prepared according to different included angles between the normal direction of the bedding plane and the axial direction of the rock sample (Φ25 mm ×50× 50 mm), and the included angle was set as the bedding angle β. The bedding plane angles of the experimental rock samples were 0°, 15°, 30°, 45°, 60°, 75°, and 90°, respectively. There were three rock samples for each angle. A total of 21 rock samples were used for the experiment. Figure 2 shows a few experimental samples with different bedding angles.

3. Microstructural Anisotropy

Figure 3 shows the SEM scanning results of the Longmaxi Formation shale used in the experiment under different bedding plane directions and different scales. It is evident from Figures 3(a)–3(d) that the microstructure plane is relatively flat in the direction parallel to the bedding plane, various mineral particles are arranged regularly, and microfractures and micropores are not developed. In Figure 3(a), microfractures are filled in the direction parallel to the bedding plane. A few dry fractures can be observed in Figures 3(b) and 3(c). These may be formed by clay precipitation after water enters the shale or during diagenesis. It is also evident from Figures 3(b) and 3(d) that there are dispersed pyrite and berry pyrite in the direction parallel to the bedding plane. The irregular shapes that can be observed in Figures 3(e)–3(f) are arranged in a disorderly manner in the direction perpendicular to the bedding plane. Furthermore, there are relatively developed micropore structures. The shapes and types of pores and fractures are more diversified and can be distinguished more clearly.

To summarize, the microstructure is not developed in the parallel bedding direction. However, there are relatively developed microfractures and micropores in the vertical bedding direction. This is mainly due to the dissolution of rocks above the bedding plane direction, which is mainly due to the filling of calcite, siderite, and clay minerals parallel to the bedding plane direction. The internal stress is concentrated in the normal direction of the bedding plane, leading to the development and extension of cracks in that direction. It can be concluded that anisotropy caused during deposition is an inherent feature of shale. Meanwhile, water can enter the rock straightforwardly along the microfractures or bedding planes owing to the unique layered characteristics and microstructure of shale. This would cause hydration and damage the integrity of the shale. In severe cases, it can cause complex problems downhole, such as borehole wall falling and collapse.

4. Acoustic and Mechanical Anisotropy

4.1. Anisotropy Analysis of Acoustic Time Difference. The standard rock samples with different bedding angles were tested for P-wave and S-wave transmission. The center emission frequency of the acoustic transducer is 260 kHz. Figure 4 shows the schematic diagram of ultrasonic testing and the variation of acoustic velocity with the bedding angle of the Longmaxi Formation shale sample. Both P-wave and S-wave time differences show a decreasing trend with the increase in β. The acoustic time difference is minimum (the acoustic velocity attains the maximum) when $\beta = 90°$. This may be owing to the anisotropy of acoustic wave propagation caused by the unique lamellar microstructure of shale. For example, interlayer fractures or a weak mudstone interlayer alter the propagation direction of acoustic waves from the vertical bedding plane ($\beta = 0°$) to the parallel bedding plane. With less layers passing through a unit distance, the low-speed medium decreases, the wave reflection and energy attenuation weaken, and the wave velocity increases [8]. This is consistent with the law that the acoustic velocity decreases with an increase in bedding plane penetration. This law was obtained by Hou et al. [8] and Xu et al. [13]. The sensitivity of the S-wave time difference to β is less than that of the P-wave time difference. The average reductions in the amplitudes of the S-wave and P-wave time differences are 15.04% and 20.60%, respectively. The average ratio of the P- and S-wave velocities increases from 1.64 to 1.76 with the increase in β. This indicates that the acoustic anisotropy in the study area is relatively strong. A large error may occur if the P-wave velocity is multiplied by a certain empirical value (such as 1.7) to estimate the S-wave velocity. A sufficient understanding of the anisotropy of shale is conducive to the accurate use of logging data to evaluate and analyze downhole shale mechanical parameters such that logging data can better serve the drilling and completion process.

4.2. Anisotropy Analysis of Mechanical Characteristics

4.2.1. Anisotropy Analysis of Stress-Strain Curves. After uniaxial compression testing of rock samples with different

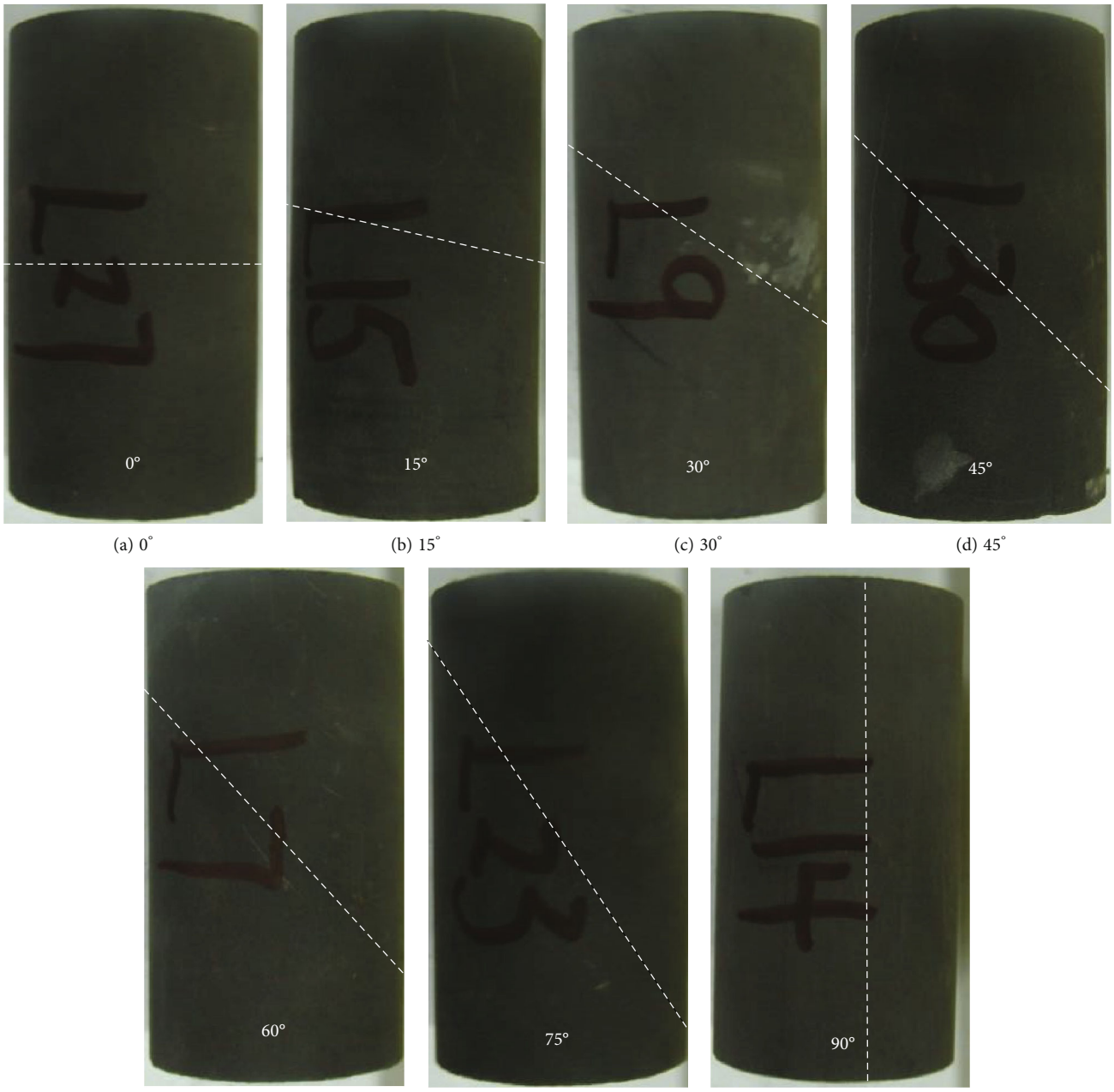

(a) 0° (b) 15° (c) 30° (d) 45°

(e) 60° (f) 75° (g) 90°

Figure 2: A few shale samples with different bedding angles.

bedding angles, the uniaxial triaxial rheometer is mainly composed of hydraulic servo system, temperature servo system, axial strain gauge, radial strain gauge, displacement sensor, data processing terminal, and PC. The testing schematic is shown in Figure 5(a). Uniaxial compression experiments under different bedding angles were performed to analyze the influence of bedding angles on mechanical parameters. A one-time continuous loading method was employed for load displacement at a rate of 0.2 mm/min. The stress and strain are monitored and recorded in real-time until the specimen breaks. The stress-strain curves are shown in Figure 5.

(1) The energy released by the rock sample after the peak value can cause the fracture to continue to expand. This indicates that the shale in the study area is hard brittle shale, which is conducive to the subsequent fracturing reconstruction

(2) The five phases of the stress-strain curves are not apparent. There is almost no pore fissure compaction phase before the elastic phase. The linear elastic deformation phase is long, and the elastic limit and yield limit almost coincide. The prepeak stress-strain curve is approximately a line segment. The

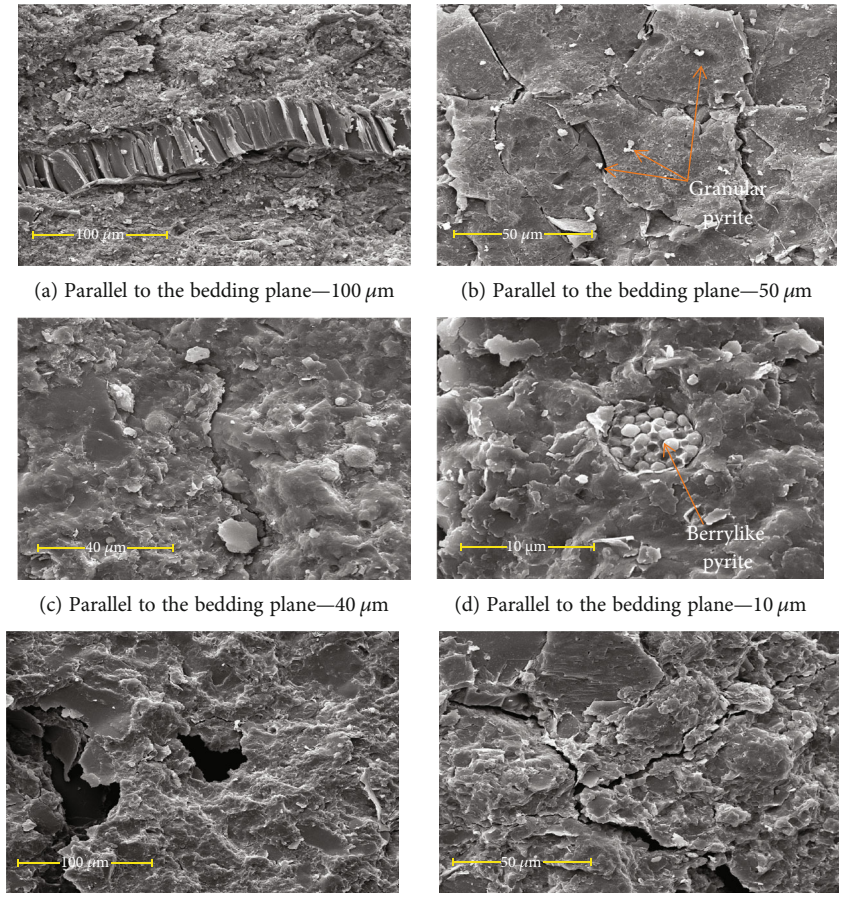

(a) Parallel to the bedding plane—100 μm (b) Parallel to the bedding plane—50 μm

(c) Parallel to the bedding plane—40 μm (d) Parallel to the bedding plane—10 μm

(e) Perpendicular to the bedding plane—100 μm (f) Perpendicular to the bedding plane—50 μm

Figure 3: SEM scanning results of shale at different scales in different bedding plane directions.

curve slope remains almost constant when the bedding angle is large. This shows a strong linear elasticity. The peak stress is caused by the discontinuity of local structure and the stress increment of primary and secondary stresses caused by the influence of local thermal stress, which can reflect the strength properties of the rock sample, the strain value at the peak stress point decreases first and then increases with the increase in bedding angle

4.2.2. Failure Mode of Rocks Sample. Shales with different bedding angles are damaged after the uniaxial compression test. Their morphology is shown in Figure 6. As a brittle rock with a bedding structure, shale shows significant anisotropy in its failure mode with different bedding plane angles.

(1) When the bedding plane angle $\beta = 0^\circ$, 15°, and 30°, the rock sample is split, and the main splitting fractures generated pass through the bedding along the axis direction. Simultaneously, the short fractures along the bedding plane connect the main splitting fractures, which are parallel to each other. This may be because the included angle of the bedding plane is small. The bedding plane is mainly subjected to compressive stress when the two ends of the rock sample are loaded under stress. Consequently, shear failure would not occur along the bedding plane. The shale is relatively brittle. In case of failure, when the splitting fracture crosses the bedding plane, it would destroy the bedding plane and generate short fractures connecting the splitting fracture

(2) When $\beta = 45^\circ$, the rock sample is subject to shear failure. Consequently, an individual shear fracture is generated along the bedding plane. This occurs because the rock sample slips directly along the bedding plane

(3) When $\beta = 60^\circ$ and 75°, the rock sample undergoes splitting failure through the rock sample and shear failure along the bedding plane. This occurs because when the axial stress is loaded, the rock sample also slides along the bedding plane to cause shear failure, whereas splitting failure occurs owing to axial compression

(4) When $\beta = 90^\circ$, the rock sample undergoes splitting failure. This results in splitting fractures along the bedding. This occurs because when the axial stress is loaded, the rock sample is compressed axially and expands radially to generate tensile stress,

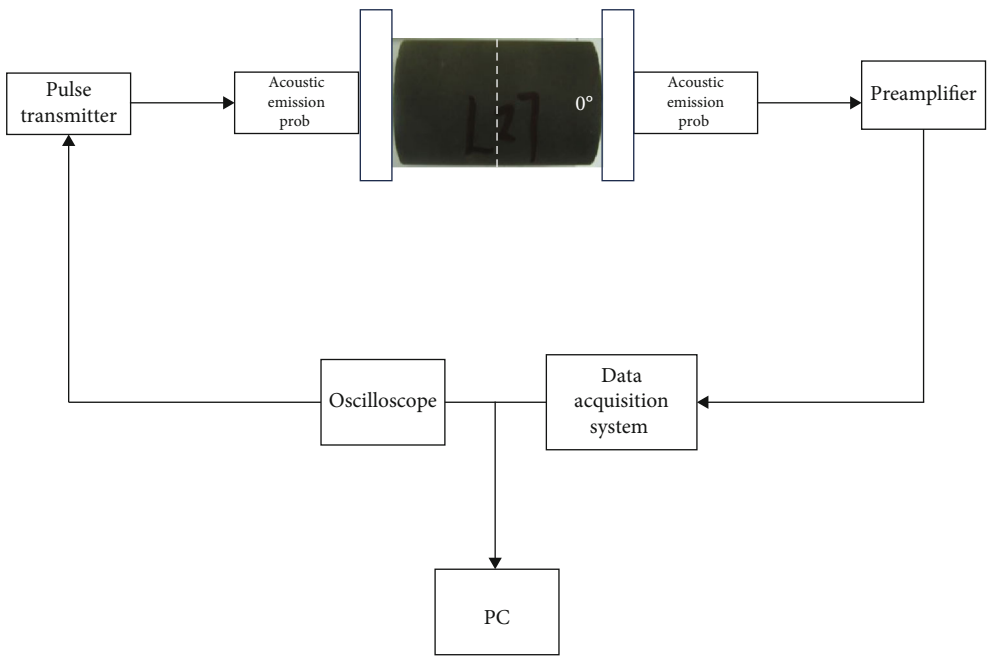

(a) Schematic diagram of ultrasonic testing

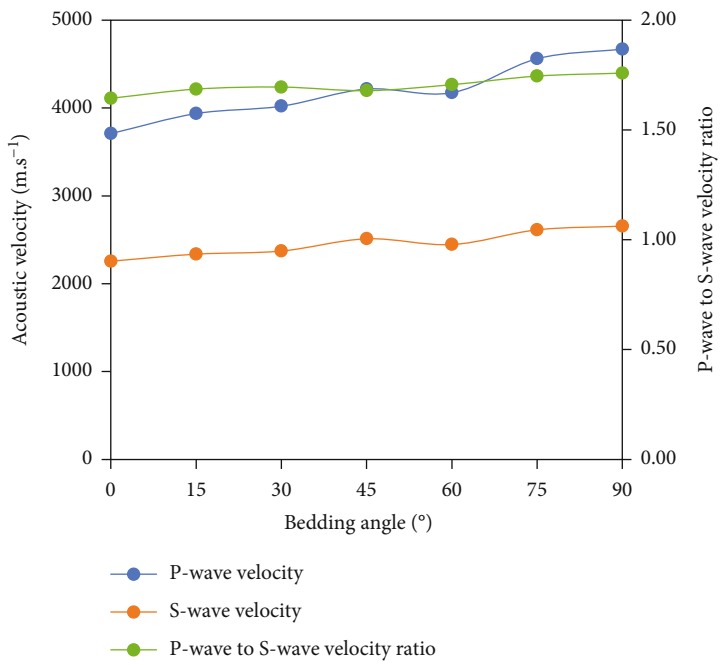

(b) Rock sample acoustic velocity

Figure 4: Ultrasonic testing and sound wave velocity.

whereas the bedding plane is cemented weakly to form multiple splitting failure planes parallel to the bedding plane

4.2.3. Anisotropy Analysis of Mechanical Parameters. After the uniaxial compression mechanical experiment on the test sample, the corresponding rock mechanical parameter characteristics are obtained. The rock mechanical parameters vary with the variation in bedding angle. This indicates that the rock mechanical parameters have strong anisotropy, which is seen in Figure 7.

The test results for compressive strength are shown in Figure 7(a). It is evident that the uniaxial compressive strength varies following a "V" shape with the variation in bedding angle. In other words, it decreases first and then increases. The compressive strength is higher when β is approximately 0° and 90°, with average values of 113.2 and 115.35 MPa, respectively. When $\beta = 60°$, the compressive

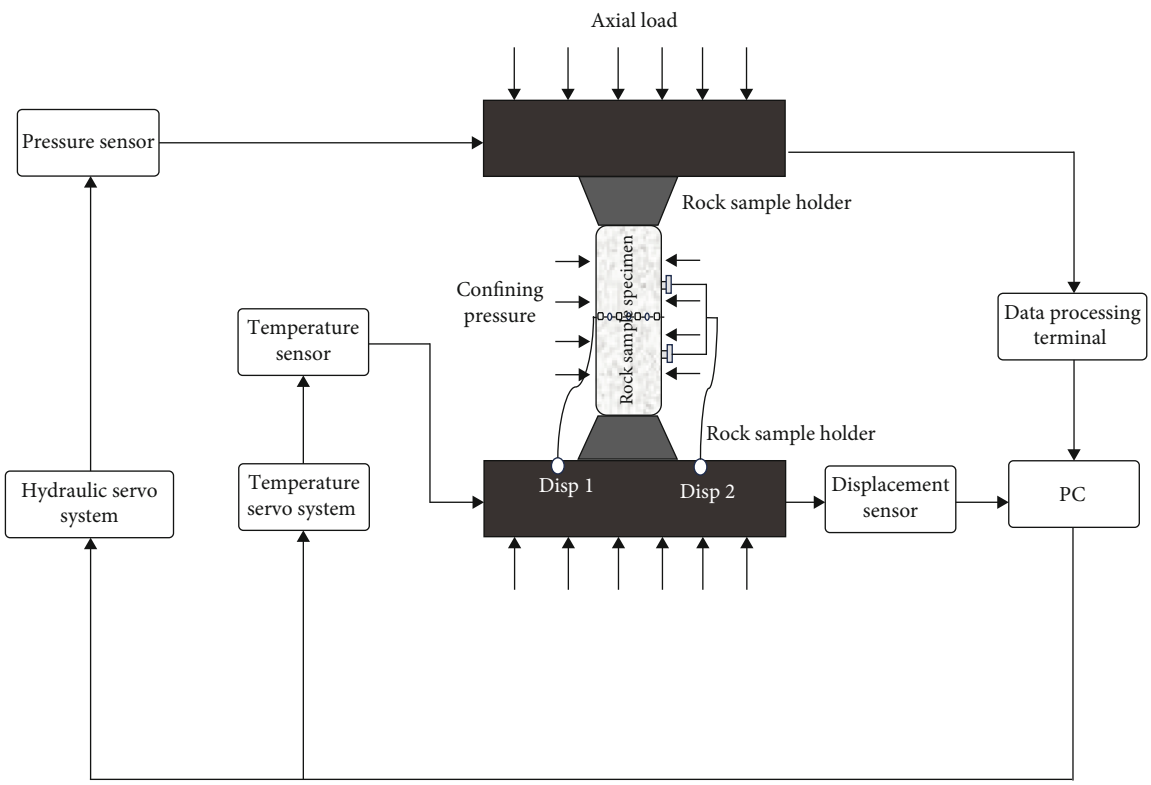

(a) Single triaxial rheological tester

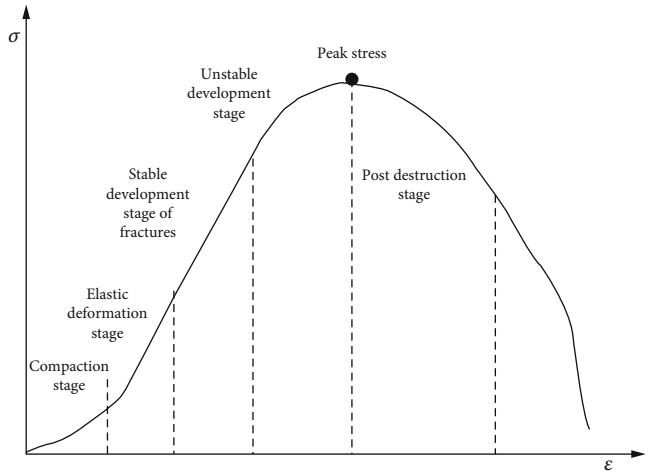

(b) Full stress-strain process curve

Figure 5: Continued.

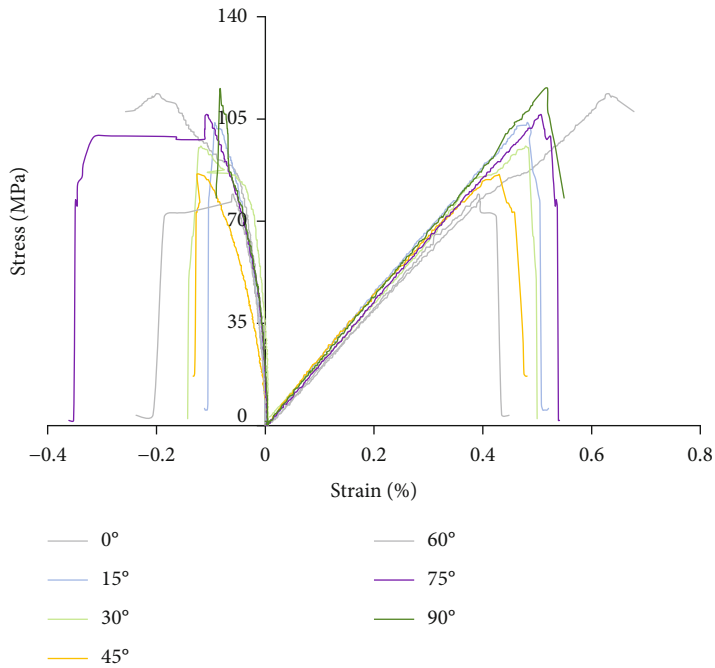

(c) Stress-strain curves

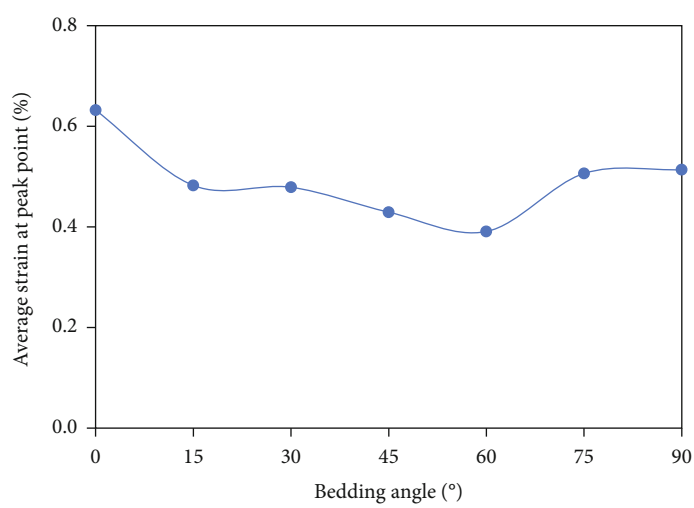

(d) Strain at peak point

Figure 5: Deformation characteristics of certain shale samples from Longmaxi Formation.

strength is minimum and the average value is 78.99 MPa. Hou et al. [8] performed a uniaxial compression test of the Longmaxi Formation shale in Pengshui. They found that the minimum value of compressive strength is attained when the bedding plane angle β is 60° and 45°. Yao et al. [22] concluded that the minimum compressive strength is obtained when $\beta = 60°$ in a uniaxial compression study of Longmaxi Formation in the south of Chongqing. Heng et al. (2015) conducted uniaxial and triaxial compression tests on Longmaxi Formation shale. They observed that both uniaxial compressive strength and triaxial compressive strength were minimal when $\beta = 60°$. Chen et al. [6] studied the anisotropy of the black shale in the Niutitang Formation of the Lower Cambrian. They conjectured that the bedding angle of the shale with the minimum uniaxial compressive strength is 60° when the confining pressure of the shale is 0, 30, and 40 MPa, and that of the shale with the minimum compressive strength is 45° at 10 and 20 MPa. Thus, the bedding angles for obtaining the minimum compressive strength differ with area and confining pressure. This angle cannot be generalized and is approximately 45° or 60°.

The elastic modulus increases gradually with the increase in β. This is consistent with the variation trend of elastic modulus obtained by Hou et al. [8] during the uniaxial compression test of Pengshui Longmaxi Formation shale. Heng et al. (2015) conducted uniaxial and triaxial compression tests (with confining pressures of 10, 20, and 30 MPa) and arrived at a similar conclusion. Although the elastic modulus

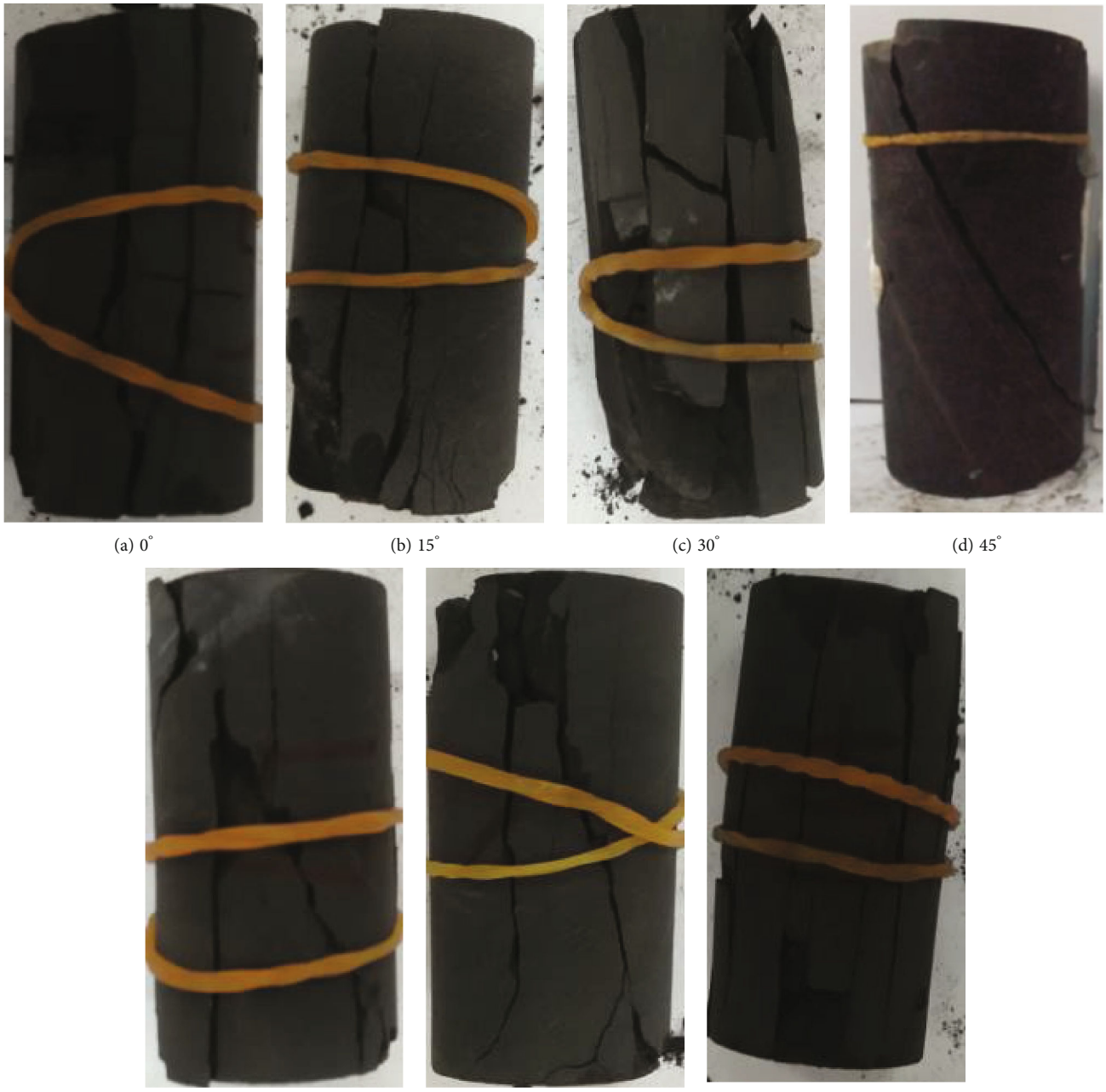

(a) 0° (b) 15° (c) 30° (d) 45°

(e) 60° (f) 75° (g) 90°

Figure 6: Failure mode of certain Longmaxi Formation shale samples.

of each rock sample does not increase with the increase in β in this experiment, the general trend is still an increase. This indicates the strong anisotropy. Poisson's ratio first decreases and then increases with the increase in β. Poisson's ratio decreases gradually when β is 0°–60° and increases rapidly when β is 60°–90°. The minimum and maximum values are obtained at 60° and 90°, respectively. Heng et al. (2015) also obtained the minimum Poisson's ratio when β was 60° in a uniaxial compression experiment of Longmaxi Formation shales.

4.3. Anisotropy Analysis of Energy Evolution Characteristics. Omitting the heat energy generated by the temperature variation, the internal energy of rock samples in the uniaxial compression test originates mainly from the work done by external forces. Part of this work done is stored in the rock in the form of elastic potential energy. The other part is dissipated when it is used for fracturing the internal structure of the rock. The total energy, elastic energy, and dissipation energy of shale samples at different phases with different bedding angles can be calculated according to the uniaxial experimental data. Figure 8 shows the energy-strain curves and axial stress-strain curves at different bedding angles. It is evident from Figure 8 that with the increase in axial stress, the strain increases, the external force continues to do work, and the total energy, elastic energy, and dissipated energy of

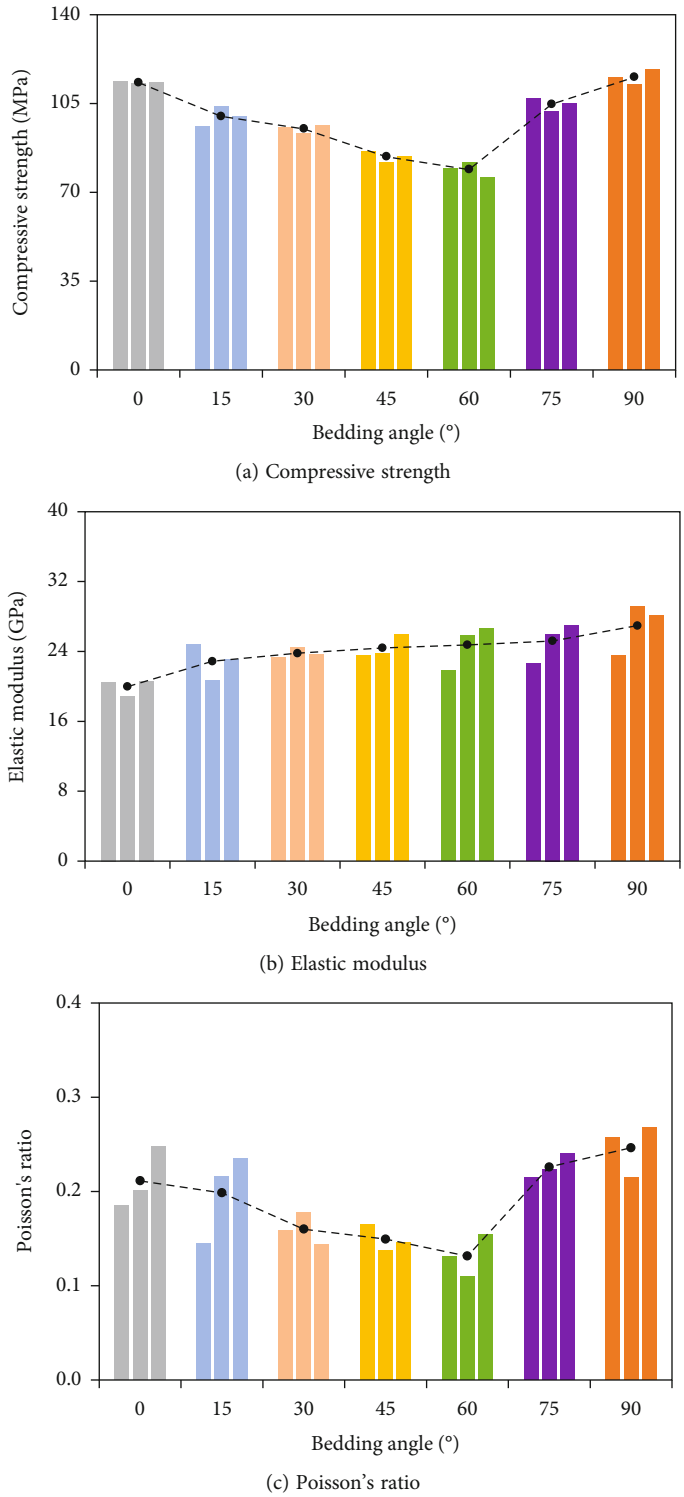

Figure 7: Characteristics of rock mechanical parameters of certain shale samples from Longmaxi Formation.

the rock sample increase. On the one hand, the elastic energy, driving energy, and fracture capacity increase. On the other hand, the increase in dissipative energy results in the formation of microfractures and fracture coalescence in the rock sample. This gradually damages the structure, reduces the bearing capacity, and decreases the energy storage limit of the rock. Various microfractures and micropores continue to develop into macrofractures with the increase in rock deformation. This results in rock fracture.

The energy evolution can be divided into three phases according to the characteristics of the energy-strain curve and axial stress-strain curve. Phase I: At the initial phase of loading, none of the rock samples displays apparent compression. In the linear elastic phase of rock sample

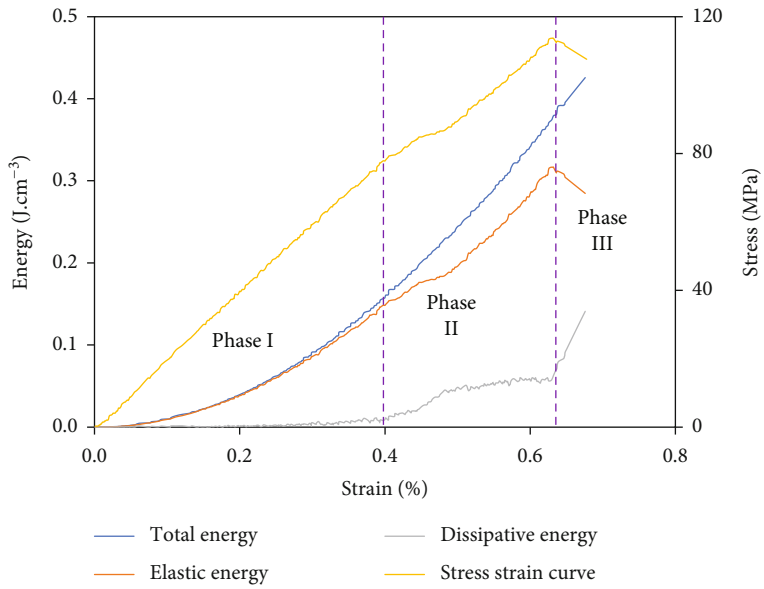

(a) $\beta = 0^{\circ}$

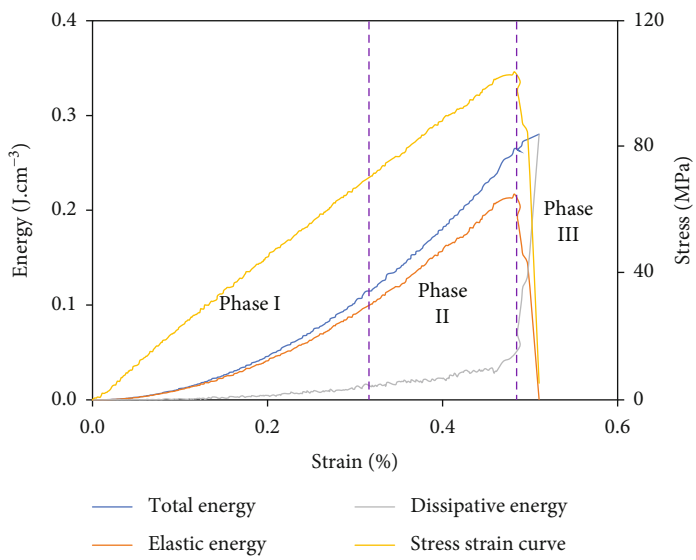

(b) $\beta = 15^{\circ}$

Figure 8: Continued.

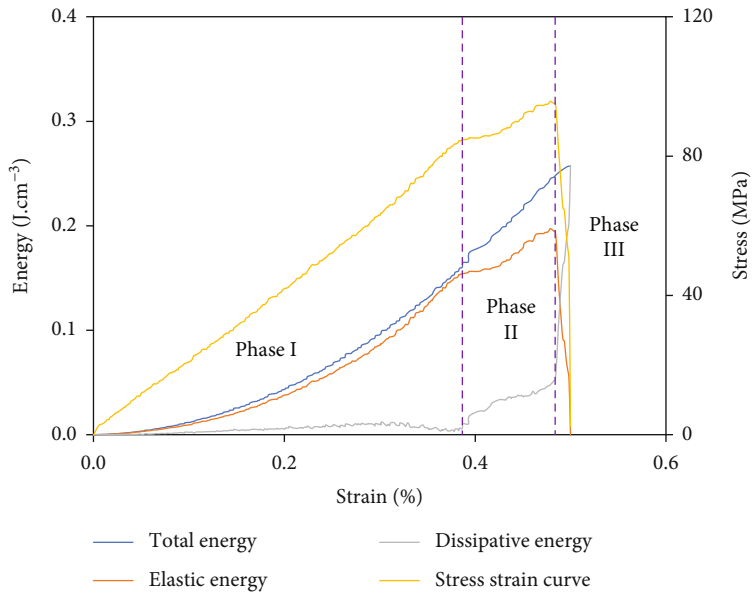

(c) $\beta = 30^{\circ}$

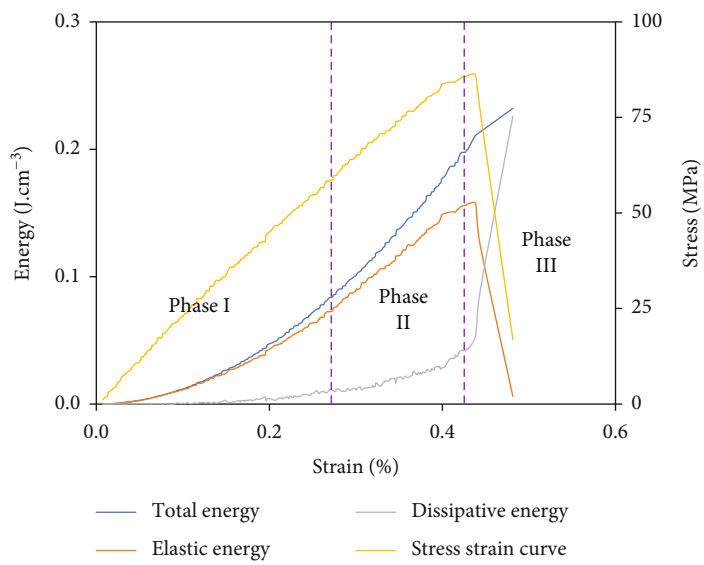

(d) $\beta = 45^{\circ}$

Figure 8: Continued.

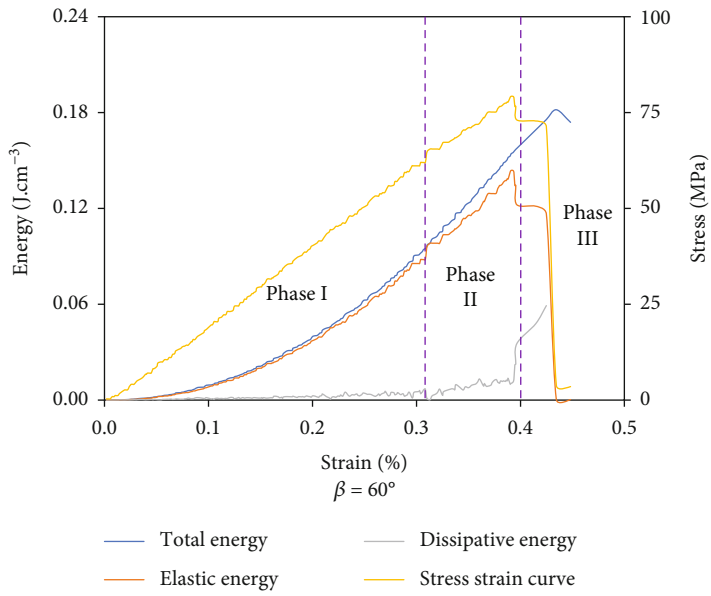

(e) $\beta = 60^{\circ}$

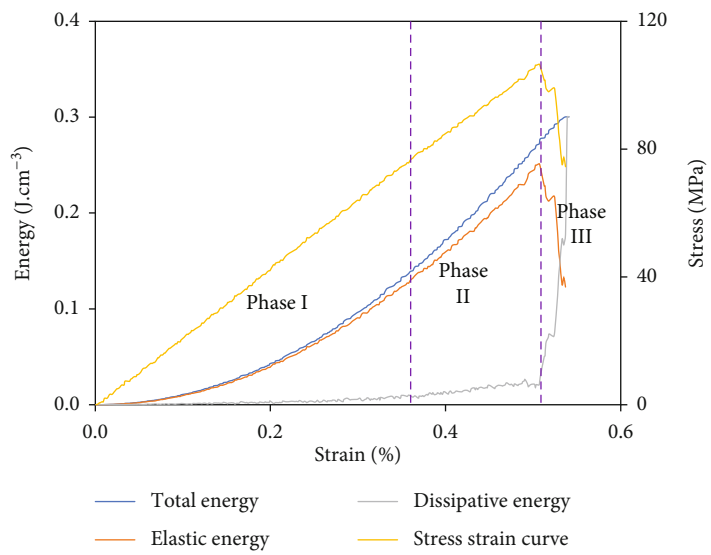

(f) $\beta = 75^{\circ}$

Figure 8: Continued.

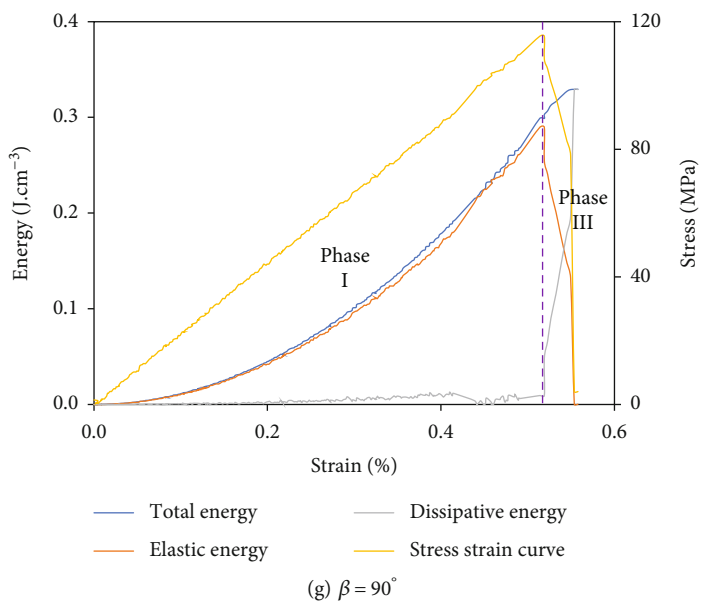

Figure 8: Energy evolution characteristics of certain Longmaxi Formation shale under different bedding angles β.

deformation, the total energy and elastic energy increase steadily, whereas the dissipated energy essentially remains unaltered. The elastic energy curve is almost parallel to the total energy curve. The shale damage is low in this phase. Phase II: The rate of increase in elastic energy reduces and the rate of increase in dissipated energy accelerates. The elastic energy curve is no longer parallel to the total energy curve. At this time, the internal fractures expand and connect with each other, thereby causing higher damage to the internal structure until the peak strength point. Phase III: At the peak strength point, the energy stored in the rock attains the maximum value that can be withstood at present, and the two attain a critical state. Subsequently, the elastic energy is released instantaneously, and the rock sample breaks.

All kinds of energy coexist throughout the entire process of rock sampling from stress to failure, but their proportions vary in different situations. The expression for its energy is as follows:

$$U = U_e + U_d. \tag{1}$$

In the formula, U, U_e and U_d, respectively, represent total energy, elastic energy, and dissipated energy (J/cm^3); σ_1 and ε_1 are axial stress (MPa) and axial strain (mm/mm), respectively.

$$U = \int \sigma_1 d\varepsilon_1 = \sum_{i=0}^{n} \frac{1}{2} (\varepsilon_{1i+1} - \varepsilon_{1i})(\sigma_{1i} + \sigma_{1i+1}). \tag{2}$$

It is evident from Figures 8(a)–8(g) that the energy evolution of rock samples differs in the same phase under the influence of different bedding angles. The rock sample with $\beta \leq 45^{\circ}$ has a more apparent Phase II compared with the rock samples with $\beta = 75^{\circ}$ and 60°. The elastic energy curve is not parallel to the total energy curve, and the dissipation energy increases to produce microfractures. Meanwhile, the rock sample with $\beta = 90^{\circ}$ does not undergo Phase II. According to the failure morphology of rock samples in Figures 6(a)–6(c) (the rock samples with $\beta = 0^{\circ}$, 15°, and 30°), during the loading deformation process in Phase II, microfractures are generated along the weak structural plane of low angle bedding, and macrofailure occurs after the peak strength point. Consequently, a short fracture connecting the splitting fracture along the bedding plane is formed. However, Phase II is not apparent for rock samples with $\beta = 60^{\circ}$ and 75°. Rock samples with $\beta = 90^{\circ}$ also do not undergo Phase II. In combination with Figures 6(e)–6(g), there are a few short fractures in the macrodamage morphology of the rock samples. The rock samples with different bedding angles also show significant differences in Phase III. For the rock samples with $\beta \leq 45^{\circ}$ and $\beta = 90^{\circ}$, macrodamage occurs after the peak strength point, and the elastic energy curve and the dissipated energy curve show smooth reduction and increase, respectively. For the rock samples with $\beta = 60^{\circ}$ and 75°, the elastic energy curve and dissipated energy curve show zigzag reduction and increase, respectively. This may be because in Phase III, the rock samples with $\beta \leq 30^{\circ}$ and $\beta = 90^{\circ}$ mainly sustain a single splitting failure, those with $\beta = 45^{\circ}$ mainly sustain a single shear failure, and those with $\beta = 60^{\circ}$ and 75° also sustain a shear failure along the bedding plane when splitting failure occurs. This may have resulted in a tortuous shape of the energy curve in Phase III.

It is evident from Figure 9(a) and Table 1 that the total energy, elastic energy, and dissipated energy at the peak strength points of different bedding angles have significant anisotropy. The variation trend of total energy and elastic energy with the increase in β is identical. It decreases first and then increases. The maximum value is obtained at 0°, and the minimum value is obtained at 60°. The dissipation

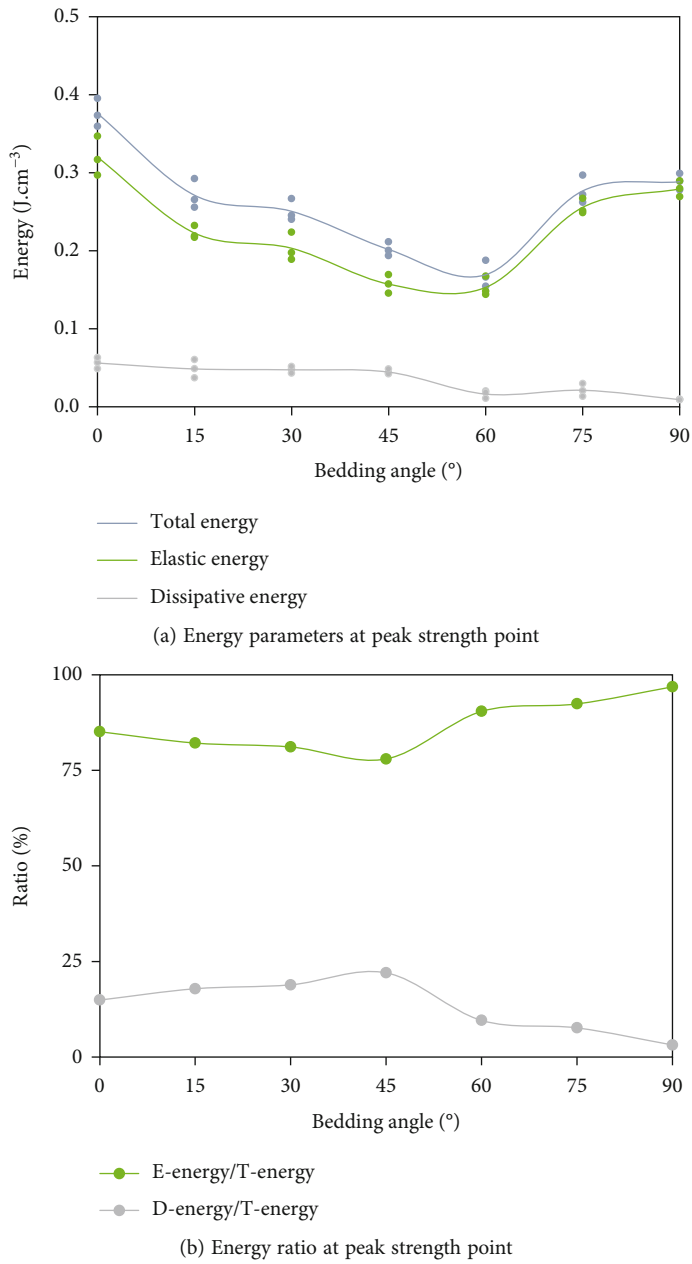

Figure 9: Variation curve of energy parameters at shale peak strength point under different bedding angles.

energy decreases with the increase in β, and the minimum value is obtained at 60°. It is evident from Figure 10(b) and Table 1 that the ratio of elastic energy to total energy decreases first and then increases with the increase in β. The maximum value of 96.83% is obtained at 90°, and the minimum value of 77.97% is obtained at 45°. The ratio of dissipated energy to total energy first increases and then decreases. The minimum value is 3.17% at 90°, and the maximum value is 22.03% at 45°. It is further explained through an analysis of the energy relationship of total energy, elastic energy, and dissipated energy at the fracture point of different bedding angles that the energy required for shale fracture at different bedding angles differs significantly. This results in the significant anisotropy of its corresponding peak strength.

5. Effect of Anisotropy on Wellbore Stability

It can be concluded based on the above analysis that shale with different bedding angles β displays spatial anisotropy. In the process of drilling horizontal wells, the included angle between the borehole axis and the normal direction of the bedding plane is numerically equal to β. In the process of drilling, the wall rocks of the vertical section, deviation section, and horizontal section of the horizontal well can be equivalent to rock samples with different bedding angles. The included angle between the axis of the wellbore and the bedding plane passing through varies many times during the process from the straight section to the horizontal section (as shown in Figure 10). In the vertical well phase,

Table 1: Energy parameters at peak strength point of shale at different bedding angles.

Bedding angle	Total energy (J/cm^{-3})	Elastic energy (J/cm^{-3})	Dissipative energy (J/cm^{-3})	E-energy/T-energy (%)AVG	D-energy/T-energy (%)AVG
	0.3731	0.3165	0.0566		
0°	0.3952	0.3465	0.0487	85.09	14.91
	0.3593	0.2965	0.0628		
	0.2653	0.2168	0.0485		
15°	0.2923	0.2322	0.0601	82.12	17.88
	0.2556	0.2188	0.0368		
	0.2451	0.1973	0.0478		
30°	0.2665	0.2236	0.0430	81.10	18.90
	0.2399	0.1886	0.0512		
	0.2002	0.1571	0.0430		
45°	0.2110	0.1691	0.0420	77.97	22.03
	0.1936	0.1454	0.0482		
	0.1542	0.1437	0.0104		
60°	0.1875	0.1673	0.0202	90.41	9.59
	0.1659	0.1479	0.0180		
	0.2716	0.2512	0.0205		
75°	0.2618	0.2486	0.0132	92.37	7.63
	0.2967	0.2670	0.0297		
	0.2989	0.2895	0.0094		
90°	0.2886	0.2795	0.0092	96.83	3.17
	0.2778	0.2689	0.0088		

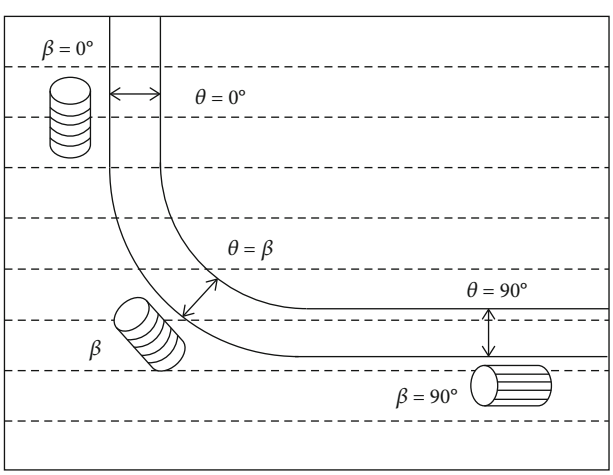

Figure 10: Angle variation law between the axial direction of horizontal well and normal direction of wall rock bedding plane in shale reservoir.

Table 2: Shale gas well-drilling data.

No.	Parameter	Value
2	Depth (m)	3198.5
2	Vertical in situ stress (MPa)	81.7
3	Maximum horizontal in situ stress (MPa)	93.2
4	Minimum horizontal in situ stress (MPa)	78.5
5	Pore pressure (MPa)	57.57
6	Biot coefficient	0.71
7	Cohesion (MPa)	8.67
8	Internal friction angle (°)	40.69
9	Cohesion of weak plane (MPa)	5.42
10	Internal friction angle of weak plane (°)	38.23

drilling is perpendicular to the horizontal bedding direction. This is equivalent to $\beta = 0°$ while coring. In the deviation phase, the included angle between the axis of the wellbore and the normal direction of the bedding plane is θ (the included angle between the wellbore direction line and the vertical direction), which is equal to β. In the horizontal well phase, the axis of the wellbore is parallel to the bedding plane, and both β and θ are 90°. The vertical section, deviation section, and horizontal section of the horizontal well satisfy the rule that the included angle between the principal stress of wall failure and the normal direction of the bedding plane is equal to the well deviation angle.

The geomechanical parameters of the formation are obtained from the drilling data of the oilfield, as shown in Table 2. Ding et al. [23] showed that the anisotropy coefficient of elastic modulus increases from 0.6 to 1.0 (the higher the value, the higher the difference, and the higher the anisotropy) by varying the elastic modulus of parallel

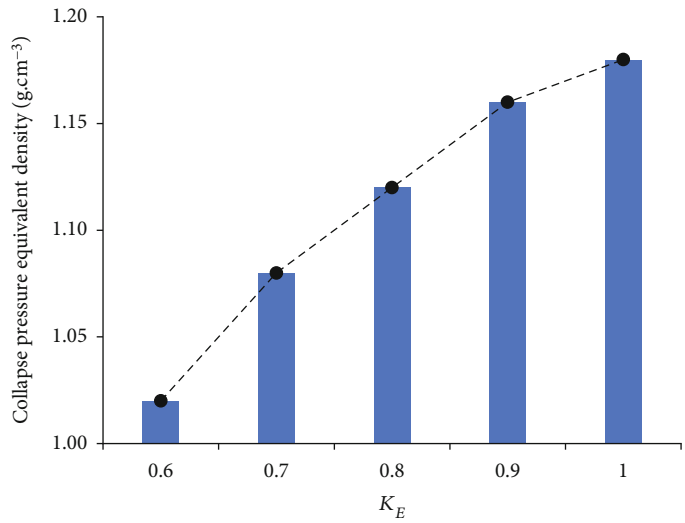

Figure 11: Effect of anisotropy on formation collapse pressure.

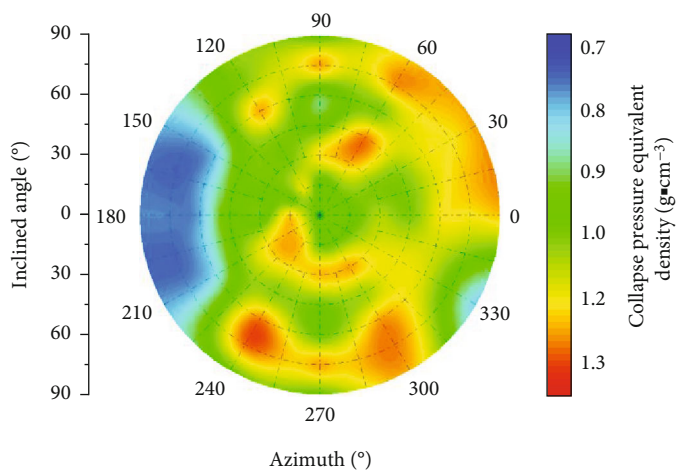

Figure 12: Distribution of formation collapse pressure under different well trajectories.

bedding while maintaining the elastic modulus of vertical bedding constant. The wellbore collapse pressure is calculated using the weak surface structure criterion. The calculation process is detailed in reference to Ding et al. [23]. The calculation results are shown in Figures 11 and 12.

$$K_E = \frac{E_h}{E_V}, \tag{3}$$

where K_E is the anisotropy of elastic modulus and E_V and E_h are the elastic moduli of the vertical bedding and parallel bedding, respectively.

Figure 11 shows the influence of anisotropy on the formation collapse pressure. It is evident from the figure that the formation collapse pressure increases with the increase in the anisotropy coefficient. This indicates that the higher the formation anisotropy, the more vulnerable is the wellbore to instability. According to the previous research, the shale strength varies with the variation in bedding angle. This results in the variation in formation collapse pressure. The comparison between the formation collapse pressures of different well paths is shown in Figure 12. It is evident from the figure that owing to the development of stratigraphic bedding planes, the distribution of collapse pressure under any borehole trajectory is not symmetric (i.e., the collapse pressure is not completely controlled by in situ stress) unlike homogeneous formation conditions. Furthermore, the distribution of high collapse pressure areas is relatively discrete, which increases the difficulty of borehole trajectory design.

The mechanical test results show that the mechanical strength of bedded shale displays significant anisotropy. Moreover, the mechanical strength between the bedding planes is low, which is a weak structural plane. The variation in mechanical strength is related to the angle between the failure principal stress direction and the normal of the bedding plane. It can be concluded that the wellbore stability

during the process of drilling horizontal wells is closely related to the strength of shale with bedding angle β. The mechanical strength of the wellbore in the vertical and horizontal sections is high, and the stability is good. The wellbore instability is most likely to occur in the deviation phase.

6. Conclusion

In this paper, taking the Longmaxi Formation shales in the southern area of the Sichuan Basin as the research object, the acoustic and mechanical anisotropy characteristics of shales are studied through various experiments, including scanning electron microscopy, ultrasonic pulse transmission, and uniaxial compression experiments, and the energy evolution laws are discussed including the main conclusions as follows:

(1) The acoustic time difference, peak strength, shear strength, elastic modulus, and Poisson's ratio of shale have significant anisotropic characteristics. The time difference of P- and S-waves decreases with the increase in bedding angle. The compressive strength and Poisson's ratio decrease first and then increase with the increase in bedding angle

(2) Shale is a brittle rock with a bedding structure. Its failure modes show significant diversity with different bedding plane angles, mainly including single-splitting failure, shear failure, and shear-splitting failure

(3) According to the analysis of energy evolution characteristics, the elastic energy and dissipated energy absorbed and stored display significant anisotropy under the condition of work done by external forces. The energy evolution process is the origin of shale strength anisotropy. The total energy and elastic energy decrease first and then increase with the increase in the bedding angle

(4) While drilling horizontal wells, the wall stability of the vertical section, deviation section, and horizontal section is closely related to the shale strength variation law under different bedding angles β

Data Availability

Data is available on request from the authors.

Conflicts of Interest

The authors declare that there is no conflict of interest regarding the publication of this paper.

Authors' Contributions

Liu Xiangjun was assigned to the data analysis, writing, and reviewing. Zhuang Dalin provided substantial contributions to the experiment, writing, reviewing, and data analysis. Xiong Jian helped with data analysis, writing, and reviewing. Zhou Yishan contributed to the data analysis, writing, and reviewing. Liu Junjie was involved in the data analysis. Deng Chong worked on writing and reviewing. Liang Lixi was responsible for the data analysis. Ding Yi was involved in writing and reviewing. Jian Xuemei helped with writing and reviewing.

Acknowledgments

This research is supported by the Science and Technology Cooperation Project of the CNPC-SWPU Innovation Alliance (2020CX040201), the Natural Science Foundation of Sichuan Province (2022NSFSC1065), and the Key Project of the 22nd Extracurricular Open Experiment of Southwest Petroleum University (2022KSZ02016).

References

[1] M. Chen, Y. Jin, and Y. H. Lu, "Special topic: fundamentals of efficient oil and gas recovery in shale," *Scientia Sinica Physica, Mechanica & Astronomica*, vol. 47, no. 11, article 114600, 2017.

[2] D. Wei, Y. Zhao, H. Liu, D. Yang, K. Shi, and Y. Sun, "Where will China's shale gas industry go? A scenario analysis of socio-technical transition," *Energy Strategy Reviews*, vol. 44, article 100990, 2022.

[3] S. J. Liu, G. Gao, J. Jin, W. Gang, and B. Xiang, "Source rock with high abundance of C28 regular sterane in typical brackish-saline lacustrine sediments: biogenic source, depositional environment and hydrocarbon generation potential in Junggar Basin, China," *Journal of Petroleum Science and Engineering*, vol. 208, article 109670, 2022.

[4] C. Zou, D. Dong, Y. Wang et al., "Shale gas in China: characteristics, challenges and prospects (II)," *Petroleum Exploration and Development*, vol. 43, no. 2, pp. 182–196, 2016.

[5] P. Lyu, J. Meng, R. Pan, X. Yi, T. Yue, and N. Zhang, "Characteristics and differences analysis for thermal evolution of Wufeng–Longmaxi shale, southern Sichuan Basin, SW China," *Minerals*, vol. 12, no. 7, p. 906, 2022.

[6] T. Chen, X. Feng, X. Zhang, W. Cao, and C. Fu, "Experimental study on mechanical and anisotropic properties of black shale," *Yan Shi Li Xue Yu Gong Cheng Xue bao*, vol. 33, no. 9, pp. 1772–1779, 2014.

[7] G. Dewei, H. Honglin, L. Jun, and S. Tengfei, "Experimental study of anisotropic characteristics of a specific formation shale," *Chemistry and Technology of Fuels and Oils*, vol. 56, no. 6, pp. 971–984, 2021.

[8] Z. K. Hou, C. H. Yang, Y. T. Guo et al., "Experimental study on anisotropic properties of Longmaxi Formation shale under uniaxial compression," *Yantu Lixue/Rock and Soil Mechanics*, vol. 36, no. 9, pp. 2541–2550, 2015.

[9] B. Lei, J. P. Zuo, H. Y. Liu, J. Wang, F. Xu, and H. Li, "Experimental and numerical investigation on shale fracture behavior with different bedding properties," *Engineering Fracture Mechanics*, vol. 247, article 107639, 2021.

[10] S. Cui, H. Liu, Y. Meng, Y. Fan, J. Wang, and Z. Han, "Study on mechanical properties and wellbore stability of deep brittle shale," *Journal of Petroleum Science & Engineering*, vol. 194, article 107500, 2020.

[11] Y. Wang and C. H. Li, "Investigation of the P- and S- wave velocity anisotropy of a Longmaxi Formation shale by real-time ultrasonic and mechanical experiments under uniaxial

deformation," *Journal of Petroleum Science and Engineering*, vol. 158, pp. 253–267, 2017.

[12] Q. Chen, G. Yao, H. Zhu, Y. Tan, and F. Xu, "Numerical simulation of ultrasonic wave transmission experiments in rocks of shale gas reservoirs," *AIP Advances*, vol. 7, no. 1, article 015205, 2017.

[13] F. Xu, Q. Chen, H. Zhu et al., "Response analysis of shale bedding structure to ultrasonic characteristics and its application," *Petroleum Exploration and Development*, vol. 46, no. 1, pp. 82–92, 2019.

[14] Y. Luo, H. Gong, K. Xu, C. Pei, X. Wei, and X. Li, "Progressive failure characteristics and energy accumulation of granite with a pre-fabricated fracture during conventional triaxial loading," *Theoretical & Applied Fracture Mechanics*, vol. 118, article 103219, 2022.

[15] Y. F. Wang and F. Cui, "Energy evolution mechanism in process of sandstone failure and energy strength criterion," *Journal of Applied Geophysics*, vol. 154, pp. 21–28, 2018.

[16] Y. Xue, J. Liu, P. G. Ranjith, Z. Zhang, F. Gao, and S. Wang, "Experimental investigation on the nonlinear characteristics of energy evolution and failure characteristics of coal under different gas pressures," *Bulletin of Engineering Geology and the Environment*, vol. 81, no. 1, pp. 1–12, 2022.

[17] S. B. Chen, Y. M. Zhu, Y. Qin, H. Wang, H. Liu, and J. Fang, "Reservoir evaluation of the lower Silurian Longmaxi Formation shale gas in the southern Sichuan Basin of China," *Marine and Petroleum Geology*, vol. 57, pp. 619–630, 2014.

[18] S. B. Chen, Y. M. Zhu, H. Y. Wang, H. Liu, W. Wei, and J. Fang, "Shale gas reservoir characterisation: a typical case in the southern Sichuan Basin of China," *Energy*, vol. 36, no. 11, pp. 6609–6616, 2011.

[19] Y. Lin, S. Liu, S. Gao, Y. Yuan, J. Wang, and S. Xia, "Study on the optimal design of volume fracturing for shale gas based on evaluating the fracturing effect—a case study on the Zhao Tong shale gas demonstration zone in Sichuan, China," *Journal of Petroleum Exploration and Production*, vol. 11, no. 4, pp. 1705–1714, 2021.

[20] Q. Nansheng, L. Wen, F. Xiaodong, L. Wenzheng, X. Qiuchen, and Z. Chuanqing, "Maturity evolution of lower Cambrian Qiongzhusi formation shale of the Sichuan Basin," *Marine and Petroleum Geology*, vol. 128, article 105061, 2021.

[21] J. H. Wang, A. Q. Wu, and Q. Sheng, *GB/T 50266—2013 Test Method Standard for Engineering Rock Mass*, China Planning Publishing House, Beijing, 2013.

[22] G. H. Yao, Q. Chen, H. Liu et al., "Experiment study on mechanical properties of bedding shale in lower Silurian Longmaxi shale Southeast Chongqing," *Chinese Journal of Rock Mechanics and Engineering*, vol. 34, Supplement 1, pp. 3313–3319, 2015.

[23] Y. Ding, P. Y. Luo, X. J. Liu, and L. Liang, "Wellbore stability model for horizontal wells in shale formations with multiple planes of weakness," *Journal of Natural Gas Science and Engineering*, vol. 52, pp. 334–347, 2018.